INT. J. GEOGRAPHICAL INFORMATION SYSTEMS, 1995, VOL. 9, NO. 4, 405–419

Research Article

Topographic solar radiation models for GIS

RALPH DUBAYAH
Department of Geography, University of Maryland, College Park, Maryland 20742, USA

and PAUL M. RICH
Biological Sciences, University of Kansas, Lawrence, Kansas, 66045, USA

Abstract. Incident solar radiation at the Earth's surface is the result of a complex interaction of energy between the atmosphere and the surface. Recently much progress has been made towards the creation of accurate, physically-based solar radiation formulations that can model this interaction over topographic and other surfaces (such as plant canopies) for a large range of spatial and temporal scales. In this paper we summarize our current work on solar radiation models and their implementation within both GIS and image processing systems. An overview of the effects of topography and plant canopies on solar radiation is presented along with a discussion of various options for obtaining the data necessary to drive specific solar radiation models. Examples are given from our own work using two models, ATM (Atmospheric and Topographic Model), a model based within an image processing framework, and SOLARFLUX, a GIS-based model. We consider issues of design, including GIS implementation and interface, computational problems, and error propagation.

1. Introduction

Topography is a major factor determining the amount of solar energy incident at a location on the Earth's surface. Variability in elevation, slope, slope orientation (azimuth or aspect), and shadowing, can create strong local gradients in solar radiation that directly and indirectly affect such biophysical processes as air and soil heating, energy and water balances, and primary production (Geiger 1965, Holland and Steyn 1975, Gates 1980, Kirkpatrick and Nunez 1980, Davis *et al.* 1989, Dubayah *et al.* 1989, Brown 1991, Davis *et al.* 1992, Dubayah 1992). Although it has been recognized that topographic effects are important, until recently little has been done to incorporate them in a quantitative and systematic manner into a modelling environment (Rich and Weiss 1991, Dubayah 1992, Duguay 1993, Hetrick *et al.* 1993a, 1993b, Saving *et al.* 1993, Dubayah 1994, Rich *et al.* 1994). Several factors have limited progress on topographic solar radiation modelling including: (1) the complexity of physically-based solar radiation formulations for topography; (2) lack of data needed to drive such formulations; and (3) lack of suitable modelling tools.

A geographical information systems (GIS), running on a fast, new generation workstation, can provide the appropriate modelling platform for formulating and running sophisticated solar radiation models. Many of the necessary capabilities are now widely accessible from GIS platforms, including abilities to construct or import digital elevation models, to integrate diverse databases for input and output, to access viewshed analysis algorithms that permit assessment of sky obstruction and reflectance, and to harness the computational power required for complex calculations.

0269-3798/95 $10·00

In this paper we provide an overview of our research on solar radiation models and their implementation. We first consider topographic effects on direct and diffuse fluxes. We then outline methods for obtaining the data necessary to drive radiation models. Examples of solar radiation modelling using two existing models are presented, one of which (SOLARFLUX) is currently implemented within a GIS. We discuss design considerations, data needs, data structures, error propagation, and lastly some future directions.

2. Modelling topographic and canopy effects

Detailed descriptions of some topographic solar radiation models can be found in Dozier (1980, 1989), Dubayah *et al.* (1990), Dubayah (1992), Duguay (1993), and Hetrick *et al.* (1993a, 1993b). Here we briefly summarize the topographic effects most models should consider. Consider a terrain whose topography is represented by a grid of elevation points (a digital elevation model). At each point the elevation, slope and aspect may vary, and there may be variable shadowing and reflectance effects. The direct and diffuse irradiance incident on a level surface at a particular point must be modified to account for these modulating features of the topography.

There are three sources of illumination on a slope in the solar spectrum (figure 1): (1) direct irradiance, which is strongly influenced by illumination angle, and includes self-shadowing by the slope itself and shadows cast by nearby terrain; (2) diffuse sky irradiance, where a portion of the overlying hemisphere may be obstructed by nearby terrain; and (3) direct and diffuse irradiance reflected by nearby terrain towards the point of interest.

2.1. *Direct irradiance*

The direct irradiance is a function of solar zenith angle, solar flux at the top of the atmosphere (exoatmospheric flux), atmospheric transmittance or optical depth, solar illumination angle on the slope, and sky obstruction. Zenith angle and exoatmospheric flux vary by date, while optical depth is a function of atmospheric absorbers and

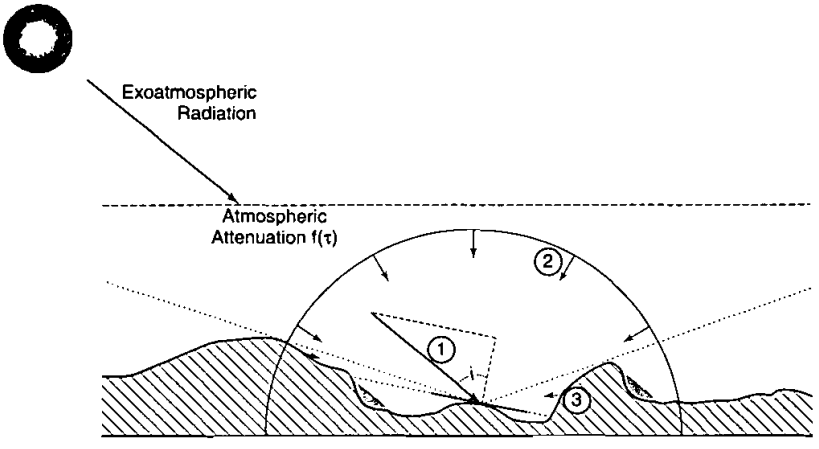

Figure 1. The three sources of solar radiation on a slope: (1) direct irradiance; (2) diffuse irradiance from the sky, where a portion of the overlaying hemisphere may be blocked by nearby terrain; and (3) irradiance reflected off of nearby terrain. The solar illumination angle is i and atmospheric optical depth is τ.

scatterers and can vary greatly over time and space. Optical depth is also a function of elevation because pressure, and hence the number of absorbers and scatterers, decreases with height. The solar illumination angle i, is the angle the Sun's rays make with the slope normal and varies with solar zenith and azimuth angles and slope angle and azimuth. Given an optical depth of τ_0, the direct irradiance on a slope is

$$\cos i\, S_0 \exp(-\tau_0/\cos\theta_0) = [\cos\theta_0 \cos S + \sin\theta_0 \sin S \cos(\phi_0 - A)]S_0 \times \exp(-\tau_0/\cos\theta_0) \quad (1)$$

where $\cos i$ is the cosine of the solar illumination angle on the slope, S_0 is the exoatmospheric solar flux, θ_0 is the solar zenith angle, ϕ_0 is the solar azimuth, A is the azimuth of the slope, and S is the slope angle. Both S and A are derived from digital elevation data. For clear sky conditions the spatial variability of incoming solar radiation will usually be dominated by (1).

Shading is a function of how directly the Sun's rays are incident upon the slope, i.e., a function of $\cos i$. (Note: we use the term shading here in the cartographic sense, as in 'shaded relief map'). However, nearby terrain may cast shadows on the point of interest, independent of $\cos i$ for that point. We call this effect shadowing (as distinct from shading). To determine whether a point is in shadow, the zenith angle to the horizon is calculated and compared with the solar zenith angle. If the solar zenith angle is greater than the horizon angle, that point cannot see the Sun and is in shadow, and its $\cos i$ value set equal to zero. Figure 2 illustrates this difference between shading and shadowing.

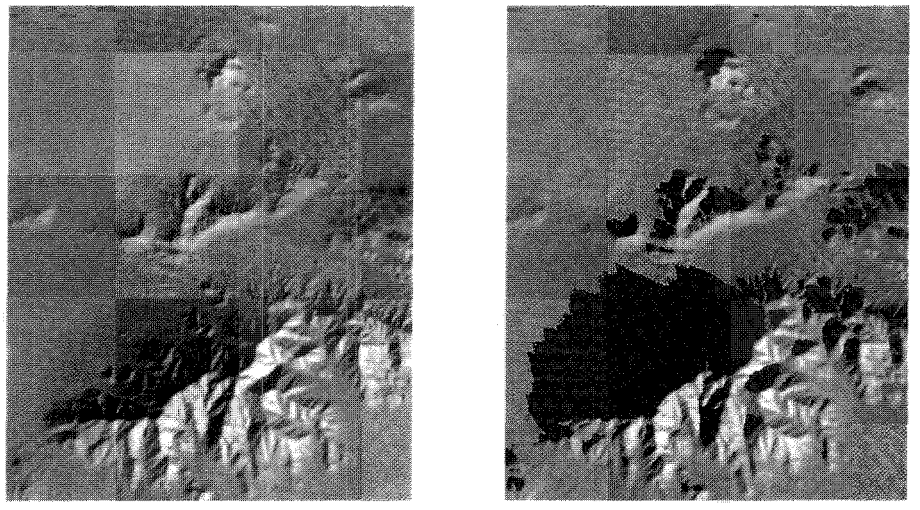

(*a*) (*b*)

Figure 2. The effects of shading and shadowing on direct irradiance. Shading is determined by the cosine of the solar illumination angle on a slope ($\cos i$). Map (*a*) gives $\cos i$ where lighter tones represent larger values of $\cos i$, and therefore larger values of direct irradiance, ranging from $\cos i = 0$ (black) to $\cos i = 1$ (white). In contrast, shadowing, the obstruction of the Sun by intervening topography, is independent of shading ($\cos i$) and is determined by comparing the horizon angle in the direction of the Sun with the solar zenith angle. Those points that cannot view the Sun are masked out from the $\cos i$ map, as shown in (*b*). The maps were generated from the U.S.G.S. 30 m DEM of the Tiefort Mountains, California, USA.

2.2. *Diffuse irradiance*

Unlike direct irradiance, exact calculation of the diffuse irradiance on a slope is difficult and almost always involves some degree of approximation. In general it is a function of solar geometry, pressure (elevation), and the scattering and absorbing properties of the atmosphere. In addition, two other factors must be considered: (1) anisotropy in the diffuse irradiance field; and (2) the amount of sky visible at a point (its sky view factor).

In general, diffuse irradiance is not isotropic, i.e., it varies depending on sky direction. Experience tells us that for clear-sky conditions this is the case, given the familiar observation of a brighter sky near the horizon and near the disk of the Sun. Modelling anisotropy can be complex, especially under cloudy or partly cloudy conditions. This is further complicated because atmospheric conditions can change rapidly. To simplify the problem we often assume that the diffuse radiation coming from the sky is isotropic. However, anisotropy can be explicitly modelled (see § 5.3 below for a brief discussion).

2.2.1. *Sky view factor*

At any given location, a portion of the sky may be obstructed by topography, thereby reducing diffuse irradiance from corresponding sky directions. Sky obstruction can result either from 'self-shadowing' by the slope itself (shading) or from adjacent terrain (shadowing). A sky view factor V_d can be calculated that gives the ratio of diffuse sky irradiance at a point to that on an unobstructed horizontal surface. In theory, the diffuse flux should be calculated by multiplying the sky view factor in a particular direction by the amount of diffuse irradiance in that sector of the sky, and integrating over the hemisphere of sky directions. This is computationally complex and storage intensive because it requires the calculation of V_d and diffuse irradiance for each sky sector and for each grid point. If we assume that diffuse irradiance is isotropic, only one view factor is associated with each grid location (as opposed to a factor for each direction). Using an isotropic assumption, the diffuse irradiance is given by

$$V_d \bar{F}\downarrow(\tau_0) \tag{2}$$

where $\bar{F}\downarrow(\tau_0)$ is the average diffuse irradiance on a level surface at that elevation, and V_d varies from 1 (unobstructed) to 0 (completely obstructed). Dozier and Frew (1990) provide details on finding V_d using horizon angles. Hetrick *et al.* (1993 a) give a highly simplified formulation for diffuse flux on a slope based on Gates (1980). Rich *et al.* (1994) outline a general framework for both isotropic and anisotropic conditions. Some GIS environments provide a 'viewshed' capability that delineates for a given point the area that can be seen from that point. However, as currently implemented, such functions are not flexible enough to be exploited directly for radiation modelling.

2.3. *Relative importance of topographic effects*

Under clear sky conditions, variability in illumination angle dominates the spatial variability in radiation maps. For example, the percentage of direct to total irradiance for mid-latitude summer conditions at sea-level is typically over 80 percent. However, as the optical depth of the atmosphere increases, diffuse irradiance becomes increasingly important, and it is the variability in sky factor that dominates the variability present in radiation maps. This is illustrated in figure 3 using a Digital Elevation Model (DEM) of the Grand Canyon. Figure 3 (*a*) is a map of $\cos i$ and depicts accurately, in the relative sense, incoming solar radiation under clear sky conditions.

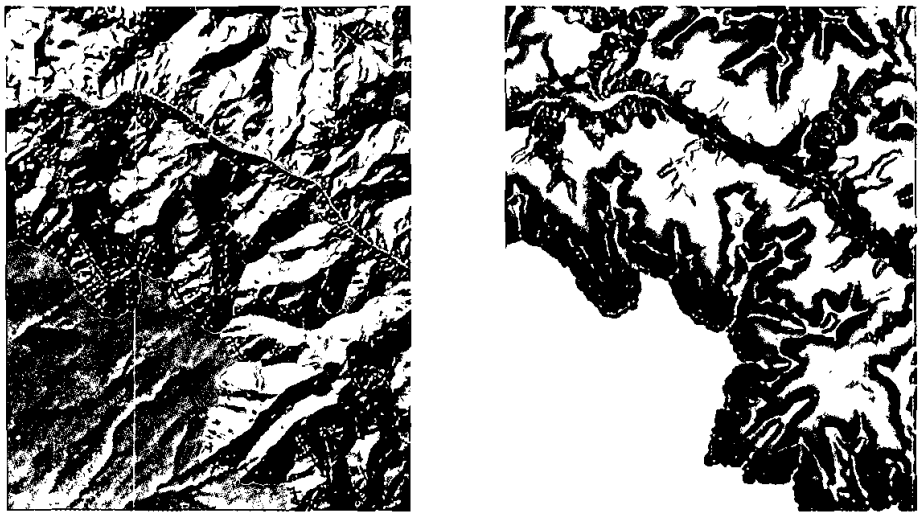

(*a*) (*b*)

Figure 3. Topographic corrections are a function of atmospheric conditions. These figures of the Grand Canyon are representative of radiation maps under (*a*) clear sky and (*b*) cloudy sky conditions. (*a*) is a map of $\cos i$, including shadows. For clear sky conditions, variability in direct irradiance, and hence $\cos i$, will dominate radiation variability. (*b*) is a map of sky view factor V_d. V_d ranges from 0 (black), to 1 (white). Lighter tones represent larger values of V_d and have less sky obstruction, as on the plateau in the bottom left of the map. As we descend deep into the canyon bottom, more sky obstruction occurs, and V_d decreases dramatically, as does the amount of incoming radiation (which is largely diffuse under overcast skies). Depending on atmospheric conditions, maps of radiation will fall somewhere between the two extremes shown. The maps were generated from the U.S.G.S. 30 m DEM of Phantom Ranch, Arizona, USA.

Figure 3 (*b*) is a map of sky view factor V_d and is representative of incoming solar radiation under overcast sky conditions, where optical depths are large and therefore the direct irradiance term close to zero. Large sky view factors (unobstructed terrain) occur on top of the Colorado Plateau, and the corresponding incoming solar radiation (which is almost entirely diffuse flux for overcase skies) is larger there. As we descend deep into the bottom of the canyon, near the Colorado River, much of the overlying hemisphere is blocked by canyon walls, and values of V_d, and therefore incoming solar radiation, decrease.

Depending on atmospheric conditions, maps of solar radiation will fall somewhere between the two extremes shown in figure 3. We emphasize that topographic effects are not independent of the atmosphere. The common notion that simple, yet fairly accurate radiation maps can be created based solely on illumination angle is not correct except under clear sky conditions. As atmospheric conditions change both the magnitude and type of topographic correction changes, reflecting the relative importance of V_d versus $\cos i$.

2.4. *Reflected irradiance*

For each point, reflected radiation from surrounding terrain must be estimated. One method of doing this is by calculating an average reflected radiation term and adjusting this by a terrain configuration factor. This configuration factor, C_t, should include both the anisotropy of the radiation and the geometric effects between a

particular location and each of the other terrain locations that are mutually visible. The contribution of each of these terrain elements to the configuration factor could be computed but this is difficult. We can again simplify by assuming (unrealistically) that the radiation reflected off of the terrain is isotropic and given that V_d for an infinitely long slope is $(1 + \cos S)/2$, approximate C_t by

$$C_t \approx \frac{1 + \cos S}{2} - V_d \tag{3}$$

The reflected radiation from the surrounding terrain is then

$$C_t \bar{F}\uparrow(\tau_0) = C_t R_0 \bar{F}\downarrow(\tau_0) \tag{4}$$

where $\bar{F}\uparrow(\tau_0)$ is the amount of radiation reflected off the surface with an average reflectance of R_0. See Hetrick *et al.* (1993 a) for a simplified formulation based on Gates (1980).

2.5. *Total irradiance on a slope*

Given the assumptions above, a physical formulation for the total irradiance on a slope can now be given as

$$E\downarrow(\text{slope}) = [V_d \bar{F}\downarrow(\tau_0) + C_t \bar{F}\uparrow(\tau_0) + \cos i \, S_0 \exp(-\tau_0/\cos\theta_0)] \tag{5}$$

where V_t, C_t and $\cos i$, are all derived from digital elevation data and all vary spatially. Since τ_0 is a function of pressure, the diffuse radiation will vary spatially with elevation, as will the direct irradiance. In practice, we specify the optical depth at a specific elevation and then calculate the change in irradiance caused solely by changes in elevation, before accounting for the other effects of terrain (the strategy employed by ATM).

Equation (5) is implicitly a function of wavelength (i.e., monochromatic). Total irradiance is found by integrating it with respect to wavelength over the desired spectral interval. However, to do this for many spectral intervals is time-consuming (and assumes knowledge of the atmospheric optical properties for each of the intervals). A good approximation is to divide the solar spectrum into two broad bands, one mainly scattering and one mainly absorbing, corresponding to the visible and near-infrared, and use equation (5) in each wavelength region.

Net solar radiation can be found by multiplying equation (5) by $(1 - R)$ where R is the spatially varying solar reflectance map and is distinct from R_0, the locally averaged solar reflectance used to approximate reflected irradiance (and perhaps multiple scattering between the surface and the atmosphere).

2.6. *Canopy effects and other complex sky obstruction*

Very near the ground, sky obstruction results from local features, in particular plant canopies, nearby terrain, or human-made structures, all of which can present a complex pattern of sky obstruction. Modelling incident solar radiation under circumstances of complex sky obstruction is essentially the same as that already described for locations on a topographic surface. Direct and diffuse components are calculated as the irradiance originating from unobstructed sky directions, integrated over the hemisphere of sky directions (Rich 1989, 1990). However, many problems remain, both in terms of modelling and measurement. Models must account for high temporal variability of sky conditions, anisotropic irradiance distributions, the geometric complexity of plant canopies, and the resulting complex patterns of reflectance (scattering) off of the many

canopy surfaces. A comprehensive analysis of sky obstruction would ideally involve detailed three-dimensional reconstruction of canopy architecture combined with viewshed analyses that account for both unobstructed irradiance through canopy openings and scattering. As for terrain models, reflected or scattered components are difficult to measure and model, and are commonly ignored because of their relatively small contribution of total irradiance. Rich *et al.* (1993 a) suggest that it may be practical to derive digital elevation models of the topographic surface of plant canopies that can be used to provide a first order estimate of nearground radiation flux and as input to more complete canopy radiance models.

3. Model drivers

3.1. *Terrain and surface reflectance data*

Topographic radiation models require data about the specific terrain of interest. In particular, digital elevation and surface reflectance data are needed. Digital elevation data are used to create the slope, aspect, sky view factor and terrain configuration maps that are used in the modelling process (Dozier and Frew 1990). Digital elevation data exist for many parts of the world at a variety of grid spacings (Wolf and Wingham 1992). The modelling purpose should determine the grid spacing of the data used. As grid spacing coarsens, topographic generalization occurs. Studies have shown that while regional radiation means may not change much with this generalization, the regional variances decrease significantly for different types of terrain (Dubayah *et al.* 1989, Dubayah and van Katwijk 1992).

It should be noted that digital elevation data need not represent terrain, but rather any arbitrary surface, such as buildings and trees. No aspect of the modelling process described here is constrained only to terrain.

Methodology for quantifying complex sky obstruction, such as from trees, using hemispherical photography is well developed (Rich 1989, 1990), however the technique is limited to locations for which high contrast hemispherical photographs can be obtained. The hemispherical photographs, taken with a camera near ground level pointing upwards, are used to directly measure which sky directions are obscured. The photographs can be taken in transects or arrays that permit examination of spatial patterns (Galo *et al.* 1992, Lin *et al.* 1992, Rich *et al.* 1993 b, Rich *et al.* 1994).

Information about the reflectance of the surface is required to compute multiple scattering between the surface and the atmosphere (if using radiative transfer to obtain the diffuse flux), the amount of radiation reflected off of nearby terrain for incoming radiation, and net solar radiation. The multiple scattering component is usually small for most surfaces other than snow and ice. Although vegetation can be bright in the near-infrared, atmospheric scattering is generally low in this region, and therefore multiple scattering effects are small. For incident solar radiation, a guess at the average albedoes for the entire modelling area in the visible and near-infrared is usually sufficient.

Surface reflectance maps are generally derived from satellite spectral observations (e.g., see Brest and Goward 1987, Dubayah 1992, Duguay and LeDrew 1992). These maps can then be used to obtain net solar radiation (Dubayah 1992).

3.2. *Radiation data*

For each location, a radiation formulation such as (5) requires an estimate of the direct and diffuse irradiance for a level surface at the corresponding elevation.

Obtaining these values can be difficult, especially for the diffuse flux. The source and type of radiative drivers used is perhaps the most important implementation issue because it determines whether the model will produce actual solar radiation fluxes for a given time and location or some type of 'potential' or relative radiation. For obtaining actual fluxes, some field data must be available, such as pyranometer data, atmospheric optical data, or atmospheric profile (sounding) data. For potential solar radiation, the state of the atmosphere need not be known and a very (or perfectly) clear sky condition is assumed.

Radiative transfer algorithms that describe the flux of energy through the atmosphere can be used to get the direct and diffuse fluxes. One common approximation to the radiative transfer problem is the two-stream method (Meador and Weaver 1980). If we have no information about the atmosphere, other radiative transfer programs, such as LOWTRAN7 (Kneizys *et al.* 1988), can be used to obtain standard atmospheric optical conditions at particular locations for particular times of year. If sounding data are available (providing information on the vertical profiles of temperature, water vapour, and pressure, among others) these data can be used in LOWTRAN7 to get more accurate fluxes.

Where pyranometer data are available, empirical formulations can be used to obtain the diffuse irradiance from global irradiance under either clear or cloudy conditions (Dubayah and van Katwijk 1992). Alternately, the pyranometer data may be used to obtain the optical properties needed to run the two-stream model via inversion, although the inversion is not unique (Dubayah 1991). Semi-empirical formulations can be used that combine known optical depths with empirically derived equations for the diffuse flux (e.g., see Gates 1980, Hetrick *et al.* 1993 a). For the purposes of comparing different locations across a landscape, it is often useful to calculate relative solar radiation under a common set of atmospheric conditions (Dubayah *et al.* 1989, Hetrick *et al.* 1993a, 1993b, Saving *et al.* 1993). In this case, the absolute magnitudes of fluxes are not important, but rather it is their values relative to one another that are of interest.

4. Examples: the ATM and SOLARFLUX models

In this section we present some examples from our own research using two different models, ATM (the Atmospheric and Topographic Model) (Dubayah 1992) whose basis is derived essentially from Dozier (1980, 1989), and SOLARFLUX (Hetrick *et al.* 1993a, 1993b). ATM is a collection of separate programs, each of which is part of the Image Processing Workbench (IPW) (Frew 1990). Although raster based, ATM is not explicitly implemented within a GIS. Because SOLARFLUX is implemented in the ARC/INFO and GRID GIS platform (Environmental Systems Research Institute, Inc., Redlands) as an ARC Macro Language (AML) program, it provides access to a broad range of GIS capabilities. SOLARFLUX has been used effectively in planning, conservation, microclimate and basic ecology studies (Rich *et al.* 1992, 1993a, Saving *et al.* 1993, Weiss and Weiss 1993).

4.1. *ATM*

Because it is a collection of UNIX-based tools, ATM is modular and portable. Complex functions can be created by combining individual programs using UNIX shell scripts. This in turn allows for easy interfacing at almost any point in the modelling stream. Since it is not run within a particular environment (such as ARC/INFO) there is none of the associated overhead and resulting loss of performance. Georeferencing and variable precision calculation are available. Lastly, the model has been validated

with field data for both incoming and net solar radiation for the terrain of the Konza Prairie (Dubayah 1992).

One of the main objectives in the development of ATM was to provide inputs for hydrological and snowmelt models in mountainous terrain. As such, it is explicitly concerned with atmospheric radiation problems and allows for different radiative drivers and interfaces. Using existing data, ATM can generate detailed topoclimatologies for large areas at arbitrary time intervals. A good example of this is our modelling efforts in the Rio Grande River basin of Colorado (Dubayah and van Katwijk 1992, Dubayah 1994).

A mosaic of 39 digital elevation models at 30 m grid spacing was created covering the upper portion of the basin, above Del Norte, Colorado, and west to the continental divide. A 4 year time series of hourly pyranometer measurements of direct and diffuse fluxes were available for four hydrological years beginning in 1987. The pyranometer data was used with Landsat Thematic Mapper satellite estimates of reflectance and NOAA estimates of snow covered area to create a 4 year monthly climatology of incoming radiation for the entire basin. Figure 4 shows a map radiation for the month of June 1990 for the entire basin. The highest regions at the western end of the basin are still snow covered and hence have low net radiation values because of high surface reflectance. Note that the reflectance features of the surface are barely visible; rather it is topography that dominates the spatial variability.

4.2. *SOLARFLUX*

SOLARFLUX uses input of a topographic surface, specified as a GRID of elevation values, as well as latitude, time interval for calculation, and atmospheric conditions (transmittivity), and provides output of direct radiation flux, duration of direct radiation, sky view factor, hemispherical projections of horizon angles, and diffuse radiation flux for each surface location. Applications of SOLARFLUX have spanned very different temporal and spatial scales. At the landscape, SOLARFLUX is being used to drive landscape level microclimate based habitat models for topographically diverse regions (Hetrick *et al.* 1993a, 1993b, Saving *et al.* 1993). Potential clear sky solar radiation flux can readily be calculated for any day of the year, for example the winter solstice at the Big Creek Reserve in California (figure 5). At the scale of individual trees in semi-arid woodlands (Rich *et al.* 1993 a), SOLARFLUX has been used to examine microclimate heterogeneity as it affects sites where young shrubs and trees can become established (figure 6).

5. Design considerations

5.1. *Implementation within GIS*

Because of the broad range of applications of solar radiation models, GIS developers should be encouraged to integrate basic solar radiation modelling capabilities as part of their software. Through running SOLARFLUX as an AML has the considerable advantage that it can be customized for a particular application, its performance suffers because many of the routines called from the ARC interpreter take much time to load and run. This can easily be remedied by optimizing and compiling the calculation intensive steps, such as viewshed analysis, while preserving as much flexibility as possible, for example permitting the user to specify how many sky sectors are examined. Furthermore, many of the fundamental software routines are not currently available as part of AML, and therefore have been written as customized code called from AML.

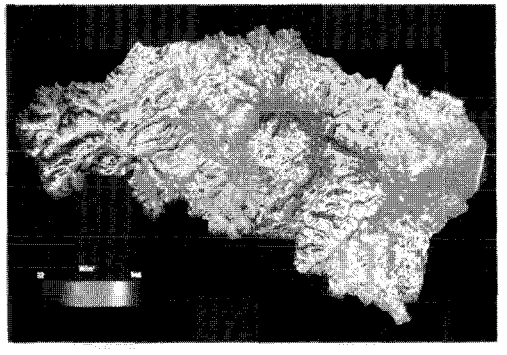

Figure 4.

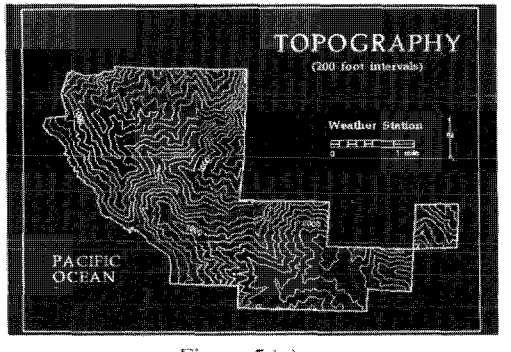

Figure 5 (*a*).

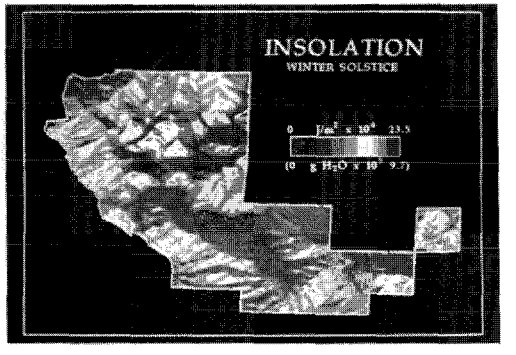

Figure 5 (*b*).

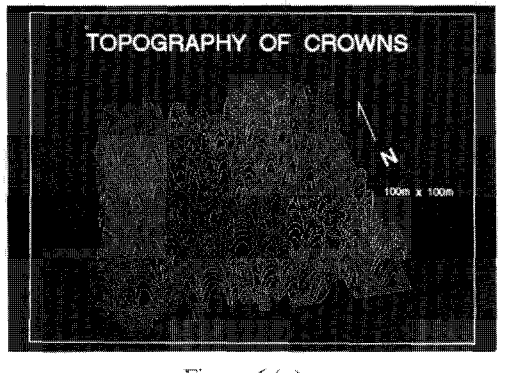

Figure 6 (*a*).

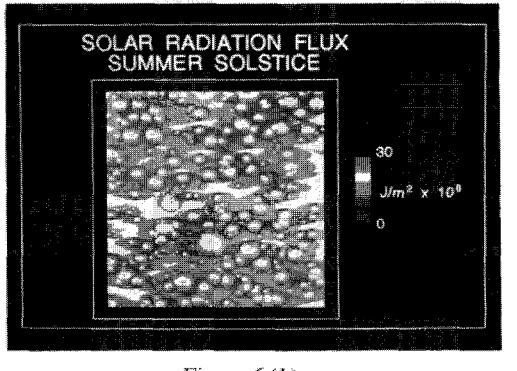

Figure 6 (*b*).

The design challenge is to provide the fundamental set of tools to model direct, diffuse, and reflected components of solar radiation without sacrificing the ability to customize the inputs, outputs, and precision of calculation.

5.2. *Interface with outside programs*

Our own experience is that an ineffective interface is a serious design flaw that discourages modellers from using GIS. A GIS-based radiation model should have the ability to easily interface with other programs, such as radiative transfer code, at any point in the modelling stream. For example the ATM model allows the user to specify the same model atmospheres included in LOWTRAN7. It then finds the range of elevations in the DEM, runs LOWTRAN7, and produces a lookup table of diffuse and direct fluxes over the range of elevations. The ability of ATM to interface with these programs is critically linked to its overall design structure. Specifically, the decoupling of elevation from other topographic effects allows for a mid-stream modelling interaction with radiative transfer programs.

Likewise, input and output data structures should facilitate interaction with applications programs, such as energy and water balance models. The conversion of final radiation maps generated within a GIS environment into a portable form suitable for use outside the environment must be both efficient and precise.

5.3. *Computational problems*

The major computational problems concern the calculation of the sky view and terrain configuration factors and canopy interactions, although this is not an issue if simple approximations are used. For example, calculation of the sky view and terrain configuration factors takes about 15 min for a 1024×1024 grid on a fast workstation.

Figure 4. Net solar radiation for June 1990. North is towards the top. The range of radiation values on the map is from 32 W/m^2 to 346 W/m^2 (J/m^2 may be found by multiplying these values by the number of seconds in the month). The map has been histogram equalized to highlight detail, so direct comparison among colours may be misleading. The high mountains near the western edge of the map are snow covered, and therefore have low net solar radiation values (blue map tones). Note that topographic variability dominates the map, so that reference features of the surface are barely visible. The Rio Grande can be seen as a yellowish line at the mouth of the basin at the extreme east. The reddish wedge at the eastern edge is the limit of Thematic Mapper reflectance coverage and represents missing data (after Dubayah 1994).

Figure 5. (*a*) Topographic map of Big Creek Reserve, California. (*b*) Daily direct insolation on the winter solstice for the Big Creek Reserve. Calculations were performed with SOLARFLUX, using digital elevation data derived from the topographic map and assuming clear sky conditions. The differences in solar radiation on north versus south-facing slopes and canyon bottom versus ridge tops leads to a high diversity of plant assemblages (after Hetrick *et al.* 1993a).

Figure 6. (*a*) The canopy surface topology of a one hectare plot in a semi-arid pinyon-juniper woodland at the Los Alamos National Environmental Research Park, New Mexico. Surface topography was reconstructed based on maps of individual trees and assuming that crown form could be approximated as the upper half of an ellipsoid, with the height as the major axis and the crown radius as the minor axis (after Rich *et al.* 1993a). (*b*) Daily direct insolation on the summer solstice. Calculations were performed with SOLARFLUX, using the canopy surface digital elevation data and assuming clear sky conditions. Shaded areas near clumps of tress and shrubs are expected to have lower water stress and be more favourable for seedling establishment.

However, for the Rio Grande DEM mosaic discussed above, the computation time was several hours. Since the factors do not change they can be preprocessed and stored (the usual procedure when using ATM). The majority of the computation is then involved in determining shadowing and terrain reflected flux.

Anisotropy in the diffuse sky and terrain fluxes is a major difficulty because this requires that factors for individual compass directions either be calculated every time the model is run or else preprocessed. If only eight directions are considered, calculation of the factors each model run would take far too long for a large grid. However, preprocessing the factor files creates a serious storage problem. For the Rio Grande grid, the isotropic factor file (with one sky view factor and one terrain configuration factor for each grid point) is about 160 Mbytes. For an eight direction anisotropic factor file, the storage required is about 1·2 Gbytes. So we are left with the design dilemma of parameters taking too long to calculate on the fly, but being too large to preprocess and store.

In certain situations, such as when only a time integrated irradiance is needed, a highly optimized approach outlined by Rich *et al.* (1994) can be used that efficiently incorporates anisotropy into the calculations. This promising approach, however, may not be suitable for some types of dynamic process modelling, such as hourly evapotranspiration calculations, where there is a time interaction among irradiance and other variables, such as soil moisture.

5.4. *Error propagation*

There are error associated with every step of solar radiation modelling: (1) associated with the radiative transfer calculations (e.g., the two-stream approximation is no better than 10% to 15%); (2) associated with interpolating and extrapolating empirical measurements over a landscape; (3) associated with registration (between reflectance and digital elevation data); and (4) associated with approximations particular to a physical model. The most serious source of error, however, is the poor quality of most digital elevation data. For example, the U.S.G.S. 30 m DEMs have considerable noise that often produces inaccurate slopes and aspects for any given location. Therefore, not only is the gradient in error, but also the horizon angles, sky view factors and terrain configuration factors. This in turn affects both the direct and diffuse irradiance calculations. If the radiation maps are then used to drive hydrologic or energy balance models, the errors that originate with the DEM are carried very far indeed from their source. For other digital elevation data, such as created from low flying aircraft, or in the case of plant canopies, reconstructed by geometry, stand measures and aerial photos, the same cautions apply.

In areas of complex topography the range in radiation values can be large. For example, some points may be in shadow while others are directly facing the Sun. This makes it difficult to flag bad radiation values on the final radiation maps because so much variability occurs naturally. It is therefore imperative to start with high quality digital elevation data that have been checked and corrected for defects before models are run. Otherwise, DEM errors will become hopelessly convolved with other aspects of the modelling process.

Brown and Bara (1994) have suggested methods for preprocessing DEM data to remove some of the systematic error in the elevation and derived fields. However, the preprocessing itself can alter portions of the DEM which are not corrupted, leading to artifacts, such as smoothing of the data. A DEM with severe high-frequency noise is unusable at fine spatial scales for radiation modelling because the values of the gradient

field can be wildly in error at specific grid cells. The errors generated at this scale may also corrupt the radiation values at coarser scales, for example as we spatially average from grid cells to larger areas. In this case, preprocessing to remove high-frequency noise by smoothing the DEM data would allow for more accurate values are coarser grid spacings; but would then preclude any modelling at the finest grid spacing because of the elimination of real, high-frequency detail in the DEM. In general, the improvements in DEM data quality obtained through preprocessing must be evaluated relative to the data degradation generated by it, and within the context of the modelling purpose and the spatial scale of inquiry.

6. Future directions

Given the complex interactions that take place between the atmosphere, topography, and plant canopies, solar radiation models can become highly elaborate. Obtaining increasingly better estimates of actual solar radiation should not be the only goal as the models evolve. The ability to calculate either potential radiation or some type of relative radiation must be retained. This is especially true for ecological modelling. As models become more complex they can become more difficult to use, mainly because of the requirement for additional input data. Thus it is important that future models avoid this pitfall by allowing for flexibility with regards to the type of radiation calculated and the input data needed.

There are a variety of extensions that we anticipate in the near future. These include adding anisotropy to the diffuse and reflected terrain calculations and incorporating further canopy effects (Rich *et al.* 1994). One important factor, not covered so far, is clouds. Some capability for modelling broken clouds should be incorporated (Dubayah *et al.* 1993, Dubayah and Loechel 1993). This is perhaps the most critical improvement suggested because the spatial variability caused by clouds can overwhelm the topographic variability caused by even the most rugged terrain. At a local scale, incorporation of ongoing solar radiation measurements can be used to assess either the short or long-term importance of clouds (Rich *et al.* 1993 b).

Another difficult problem is modelling true three-dimensional surfaces, where there may be more than one height coordinate associated with a given spatial location (as in the case of overlapping plant canopies). Most systems cannot readily handle true three dimensional surfaces. Work is needed on the representation of such surfaces and the computation of energy transfer through them.

7. Conclusions

Whether used for hydrology or ecology, for agriculture of forestry, for conservation or management, or for engineering or design, there is no shortage of applications that require the ability to model solar radiation intercepted by complex topographic surfaces. Much of the theory is now in place, and implementation is progressing rapidly. GIS could provide the ideal modelling environment for interface of inputs and outputs of solar radiation models. Models such as SOLARFLUX and ATM serve as prototypes for a future generation of solar radiation models that should be an integral part of any GIS.

Acknowlegments

This work was supported by NASA grant NAGW-2928, NASA grant NAG 5-2358, the University of Maryland Laboratory for Global Remote Sensing Studies, the University of Kansas Research Development Fund, the Los Alamos National

Laboratory Environmental Research Park, the Kansas Applied Remote Sensing Program, and the Kansas Biological Survey. Additional support was provided by Calcomp Inc., Environmental Systems Research Institute, Inc., and Sun Microsystems, Inc. We thank William Hetrick, Sara Loechel, Shawn Saving, and Stuart Weiss for various inputs.

References

BREST, C. L., and GOWARD, S. N., 1987, Derivation of albedos from spectrally limited space sensors. *International Journal of Remote Sensing*, **8**, 351–367.

BROWN, D. G., 1991, Topoclimatic models of an alpine environment using digital elevation models within a GIS, *Proceedings of the GIS/LIS '91 Conference* (ASPRS/ACSM/URISA/AAG: Washington), vol. 2, pp. 835–844.

BROWN, D. G., and BARA, T. J., 1994, Recognition and reduction of systematic error in elevation and derivative surfaces from 7·5-minute DEMs. *Photogrammetric Engineering & Remote Sensing*, **60**, 189–194.

DAVIS, F., DUBAYAH, R., DOZIER, J., and HALL, F., 1989, Covariance of greenness and terrain variables over the Konza Prairie. *Proceedings IGARSS '89*, Vancouver, 1322–1325.

DAVIS, F., SCHIMEL, D. S., FRIEDL, M. A., KITTEL, T. G. F., DUBAYAH, R., and DOZIER, J., 1992, Covariance of biophysical data with digital topographic and land use maps over the FIFE site. *Journal of Geophysical Research*, **97**, 19,009–19,021.

DOZIER, J., 1980, A clear-sky spectral solar radiation model for snow-covered mountainous terrain. *Water Resources Research*, **16**, 709–718.

DOZIER, J., 1989, Spectral signature of alpine snow cover from the Landsat Thematic Mapper. *Remote Sensing of Environment*, **28**, 9–22.

DOZIER, J., and FREW, J., 1990, Rapid calculation of terrain parameters for radiation modeling from digital elevation data. *IEEE Transactions on Geoscience and Remote Sensing*, **28**, 963–969.

DUBAYAH, R., 1991, Using LOWTRAN7 and field flux measurements in an atmospheric and topographic solar radiation model. *Proceedings IGARSS '91, Helsinki, Finland*, 39–41.

DUBAYAH, R., 1992, Estimating net solar radiation using Landsat Thematic Mapper and digital elevation data. *Water Resources Research*, **28**, 2469–2484.

DUBAYAH, R., 1994, A solar radiation topoclimatology for the Rio Grande River Basin. *Journal of Vegetation Science*, **5**, 627–640.

DUBAYAH, R., and VAN KATWIJK, V., 1992, The topographic distribution of annual incoming solar radiation in the Rio Grand River basin. *Geophysical Research Letters*, **19**, 2231–2234.

DUBAYAH, R., and LOECHEL, S., 1993, Using GOES-derived solar radiation fields to drive topographic solar radiation models. *EOS*, **74**, 265.

DUBAYAH, R., DOZIER, J., and DAVIS, F. W., 1989, The distribution of clear-sky radiation over varying terrain. *Proceedings IGARSS '89*, Vancouver, 855–888.

DUBAYAH, R., DOZIER, J., and DAVIS, F. W., 1990, Topographic distribution of clear-sky radiation over the Konza Prairie, Kansas. *Water Resources Research*, **26**, 679–690.

DUBAYAH, R., PROSS, D., and GOETZ, S., 1993, A comparison of GOES incident solar radiation estimates with a topographic solar radiation model during FIFE. *Proceedings of the ASPRS-ACSM Annual Convention* (Bethesda, MD: ASPRS), vol. 3, pp. 44–53.

DUGUAY, C. R., 1993, Radiation modelling in mountainous terrain: review and status. *Mountain Research and Development*, **13**, 339–357.

DUGUAY, C. R., and LEDREW, E. F., 1992, Estimating surface reflectance and albedo from Landsat-5 Thematic Mapper over rugged terrain. *Photogrammetric Engineering and Remote Sensing*, **58**, 551–558.

FREW, J. E., 1990, The Image Processing Workbench, doctoral dissertation, University of California, Santa Barbara.

GALO, A. T., RICH, P. M., and EWEL, J. J., 1992, Effects of forest edges on the solar radiation regime in a series of reconstructed tropical ecosystems. *Proceedings of the ASPR-ACSM Annual Convention* (Bethesda, MD: ASPRS), pp. 98–198.

GATES, D. M., 1980, *Biophysical Ecology* (New York: Springer-Verlag).

GEIGER, R. J., 1965, *The Climate Near the Ground* (Cambridge: MA, Harvard University Press).

HETRICK, W. A., RICH, P. M., BARNES, F. J., and WEISS, S. B., 1993a, GIS-based solar radiation flux models. *Proceedings of the ASPRS-ACSM Annual Convention* (Bethesda, MD: ASPRS), vol. 3, pp. 132–143.

HETRICK, W. A., RICH, P. M., and WEISS, S. B., 1993b, Modeling insolation on complex surfaces. *Proceedings of the Thirteenth Annual ESRI User Conference* (Redlands: ESRI) vol. 2, pp. 447–458.

HOLLAND, P. G., and STEYN, D. G., 1975, Vegetational responses to latitudinal variations in slope angle and aspect. *Journal of Biogeography*, **2,** 179–183.

KIRKPATRICK, J. B., and NUNEZ, M., 1980, Vegetation-radiation relationships in mountainous terrain: eucalypt-dominated vegetation in the Ridson Hills, Tasmania. *Journal of Biogeography*, **7,** 197–208.

KNEIZYS, F. X., SHETTLE, E. P., ABREU, L. W., CHETWYND, J. H., ANDERSON, G. P., GALLERY, W. O., SELBY, J. E. A., and CLOUGH, S. A., 1988, *Users Guide to LOWTRAN7.* Report AFGL-TR-88-0177, Air Force Geophysics Laboratory, Bedford, MA.

LIN, T., RICH, P. M., HEISLER, D. A., and BARNES, F. J., 1992, Influences of canopy geometry on near-ground solar radiation and water balances of pinyon-juniper and ponderosa pine woodlands. *Proceedings ASPRS 1992 Annual Conference*, Albuquerque (Bethesda, MD: ASPRS), pp. 285–294.

MEADOR, W. E., and WEAVER, W. R., 1980, Two-stream approximations to radiative transfer in planetary atmospheres: a unified description of existing methods and a new improvement. *Journal of Atmospheric Sciences*, **36,** 630–643.

RICH, P. M., 1989, *A Manual for Analysis of Hemispherical Canopy Photography*, Report LA-11733-M, Los Alamos National Laboratory.

RICH, P. M., 1990, Characterizing plant canopies with hemispherical photography. *Remote Sensing Reviews*, **5,** 13–29.

RICH, P. M., CLARK, D. A., CLARK, D. B., and OBERBAUER, S. F., 1993 b, Long-term study of solar radiation regimes in a tropical wet forest using quantum sensors and hemispherical photography. *Agricultural and Forest Meteorology*, **65,** 107–127.

RICH, P. M., HETRICK, W. A., SAVING, S. C., and DUBAYAH, R., 1994, Viewshed analysis for calculation of incident solar radiation: applications in ecology, *Proceedings of the ASPRS-ACSM Convention* (Bethesda, MD: ASPRS), 524–529.

RICH, P. M., HUGHES, G. S., and BARNES, F. J., 1993 a, Using GIS to reconstruct canopy architecture and model ecological processes in pinyon-juniper woodlands. *Proceedings of the Thirteenth Annual ESRI User Conference* (Redlands: ESRI), vol. 2, pp. 435–445.

RICH, P. M., and WEISS, S. B., 1991, Spatial models of microclimate and habitat suitability: lessons from threatened species. *Proceedings of the Eleventh Annual ESRI User Conference* (Redlands: ESRI), pp. 59–99.

RICH, P. M., WEISS, S. B., DEBINSKI, D. A., and MCLAUGHLIN, J. F., 1992, Physiographic inventory of a tropical reserve. *Proceedings of the Twelfth Annual ESRI User Conference* (Redlands: ESRI), pp. 197–208.

SAVING, S. C., RICH, P. M., SMILEY, J. T., and WEISS, S. B., 1993, GIS-based microclimate models for assessment of habitat quality in natural reserves. *Proceedings of the ASPRS-ACSM Annual Convention* (Bethesda, MD: ASPRS), vol. 3, 319–330.

WEISS, A. D., and WEISS, S. B., 1993, Estimation of population size and distribution for a threatened butterfly: GIS applications to stratified sampling. *Proceedings of the Thirteenth Annual ESRI User Conference* (Redlands: ESRI), vol. 1, pp. 183–193.

WOLF, M., and WINGHAM, D., 1992, The status of the world's public-domain digital topography of the land and ice. *Geographical Research Letters*, **19,** 2325–2328.